ADVANCED MATERIALS TECHNOLOGIES
www.advmattechnol.de

Direct-Write Printing of Multicolor Electroluminescent Films for Stretchable Display

*Tianhao Yu, Seungse Cho, Junsang Lee, Ziheng Wang, and Chi Hwan Lee**

Electroluminescent (EL) films are promising light sources for flexible displays, wearable electronics, and soft machines. Traditional fabrication methods like thermal lamination, transfer printing, and screen printing are often labor-intensive. To address these challenges, a mask-free, fully printable alternating-current electroluminescent (PACE) film using a direct-write printing strategy is presented. This method simplifies fabrication, enhances design flexibility, and allows precise, layer-by-layer deposition without alignment issues. The multicolor PACE film, available in blue, green, and orange, reaches a thickness of ≈150 µm and achieves 180 cd m^{-2} at 6 V μm^{-1}. It stretches up to 180% and withstands 10 000 bending/stretching cycles without significant luminance loss. Compared to conventional EL devices, the approach offers similar brightness with thinner films, avoids UV-curable elastomers, and reduces equipment needs. This innovation broadens design possibilities, especially for stretchable displays, making it ideal for rapid prototyping with computer-aided design (CAD) tools.

1. Introduction

Alternating-current electroluminescent (ACEL) devices are distinguished by their simplicity, mechanical flexibility, and robustness, as they use AC voltage to activate luminescent materials embedded in elastomers.[1–4] These properties make ACEL devices ideal for a range of electronic applications, including flexible displays,[5–12] wearable electronics,[13–15] and soft robotics.[16,17] Recent efforts in ACEL device development have focused on improving their durability and stretchability to meet the demands of increasingly dynamic and flexible environments.[18,19] Traditionally, fabrication has relied on various techniques, such as thermal lamination,[20–22] transfer printing,[23–25] and especially screen printing.[26–28] While these methods have been essential to the progress of ACEL devices, they often require multiple steps and specialized equipment, such as masks, which complicates the process. Issues like mask alignment between layers lead to inconsistencies, limiting scalability, and adaptability. Additionally, these methods frequently lack the precision required for more advanced applications, highlighting the need for more efficient and accessible fabrication techniques.[29–31]

To address these challenges, we introduce a layer-by-layer direct-write printing strategy for creating a mask-free, fully printable alternating-current electroluminescent (PACE) film. Unlike other existing printing techniques, our method eliminates the need for masks. By utilizing a commercial dispenser system for the precise deposition of solution-based materials, it simplifies the fabrication process, enhances design flexibility, and resolves mask alignment issues, resulting in more consistent and reliable production. Although direct-write methods have been explored previously, such as with UV-cured elastomers, our use of thermoplastic polyurethane (TPU) enables the production of a thinner, more stretchable EL film with a total thickness of ≈150 µm. The film achieves a luminance of 180 cd m^{-2} at 6 V μm^{-1}, comparable to or better than existing devices that typically require higher voltages and thicker films.

The effectiveness of our method is demonstrated through the creation of complex EL patterns and a flexible 8 × 8 matrix within a 2 × 2 cm^2 area, capable of displaying alphanumeric characters as a proof of concept. These devices exhibit consistent luminescence with minimal intensity variation, robust durability through extensive mechanical deformation, and high flexibility. For example, the devices can be stretched up to 180% of their original length and withstand 10 000 bending/stretching cycles without significant loss of luminance. This study

T. Yu, Z. Wang, C. H. Lee
School of Mechanical Engineering
Purdue University
West Lafayette, IN 47907, USA
E-mail: lee2270@purdue.edu
S. Cho, J. Lee, C. H. Lee
Weldon School of Biomedical Engineering
Purdue University
West Lafayette, IN 47907, USA
C. H. Lee
School of Materials Engineering
Purdue University
West Lafayette, IN 47907, USA
C. H. Lee
Elmore Family School of Electrical and Computer Engineering
Purdue University
West Lafayette, IN 47907, USA

The ORCID identification number(s) for the author(s) of this article can be found under https://doi.org/10.1002/admt.202401925

DOI: 10.1002/admt.202401925

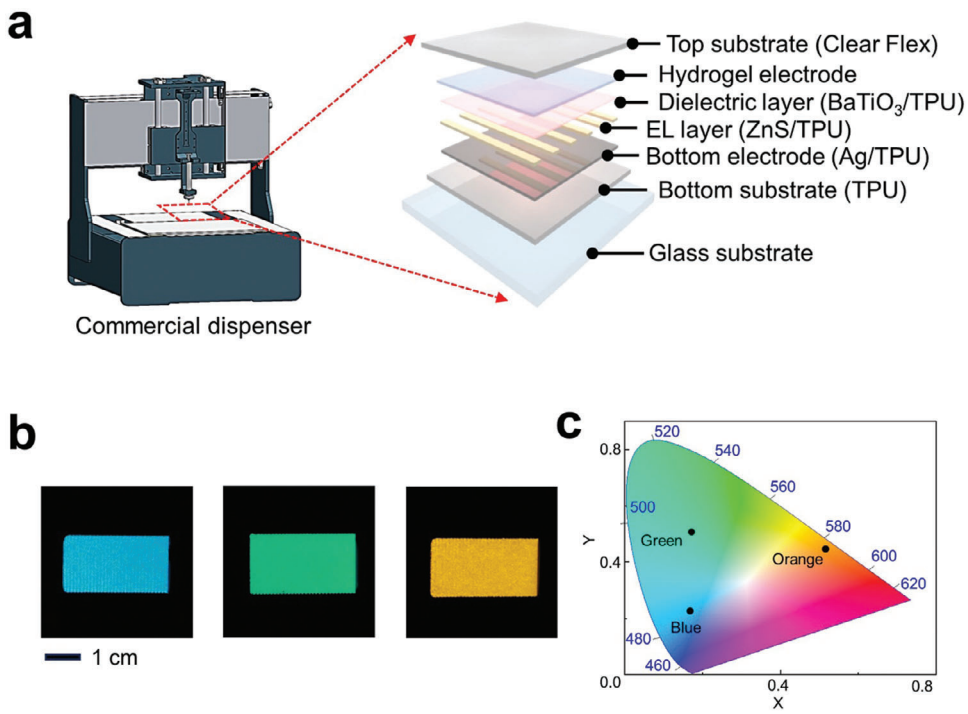

Figure 1. a) Schematic illustration of the printing process for the EL device (left) and the six-layer structure (right). b) Photographs of the multicolor EL devices. c) CIE 1931 color space chromaticity diagram showcasing EL emission in different colors, including blue, green, and orange.

introduces a transformative, fully printable fabrication strategy for flexible EL devices, paving the way for the development of advanced stretchable displays and a range of other innovative applications. By addressing the limitations of traditional printing techniques and leveraging the unique advantages of a mask-free, direct-write printing process, our work advances stretchable EL devices and opens new possibilities for their use in cutting-edge technologies.

2. Results and Discussion

2.1. Structural and Optical Characteristics of the PACE Film

Figure 1a illustrates a schematic diagram of the complete structure of the PACE film, which is fully printed using a commercial dispenser system (Nordson EFD Pro 4). Our direct-write printing technique precisely deposits functional materials in a layer-by-layer fashion, eliminating the need for complex photolithography or masking steps, thereby simplifying the manufacturing process and reducing costs. Compared to other methods, this approach allows for the creation of highly customizable and intricate device designs, enhancing mechanical flexibility and overall performance. Detailed printing parameters, materials, and fabrication processes are provided in Table S1, Figure S1, and Movie S1 (Supporting Information), respectively. The film consists of six layers arranged from bottom to top: 1) thermoplastic polyurethane (TPU) as the bottom encapsulation layer, 2) a mixture of silver flakes (Ag) and TPU as the bottom electrode layer, 3) a mixture of barium titanate ($BaTiO_3$) and TPU as the dielectric layer, 4) a mixture of zinc sulfide (ZnS) phosphors and TPU as the electroluminescent layer, 5) conductive hydrogel as the top electrode layer, and 6) Clear Flex (Smooth-On, Inc) as the top encapsulation layer. Figure 1b shows the emission of blue, green, and orange light, achieved by doping ZnS phosphors with Cu (≈0.1 wt.%), Cu (≈0.01 wt.%), and Mn (≈1 wt.%), respectively.[32] Figure 1c presents the chromaticity coordinates of the blue (0.16, 0.45), green (0.15, 0.23), and orange (0.54, 0.43) emissions according to the CIE 1931 standard color-matching system.

2.2. Viscosity and Light Emission Characteristics of the EL Layers

Figure 2a shows the measured viscosity of the EL layers prepared with different weight ratios of ZnS phosphors to TPU. The EL layers exhibit shear-thinning behavior, where viscosity decreases as the shear rate increases. The blue-highlighted region in the graph indicates the optimal viscosity range for evenly distributing EL particles. Figure 2b illustrates the illuminance as a function of various ZnS to TPU weight ratios, demonstrating that illuminance increases with higher ZnS content. This is because the embedded EL particles occupy a larger area within the TPU (Figure 2c). However, when the ZnS phosphor weight ratio reaches 3:1 w/w, the EL slurry becomes too thick, hindering consistent printing, despite the higher illuminance. Excessively aggregated EL particles may block light emission, so a 2:1 w/w ratio was chosen for the EL layer formulation (Figure S2, Supporting Information). Figure 2d presents the ON/OFF states of the PACE film, where, under AC voltage, injected hot carriers in the ZnS phosphors achieve high speeds due to the electric field and undergo impact ionization, resulting in radiative relaxation of luminescent centers and light emission at wavelengths determined by the ZnS dopants.

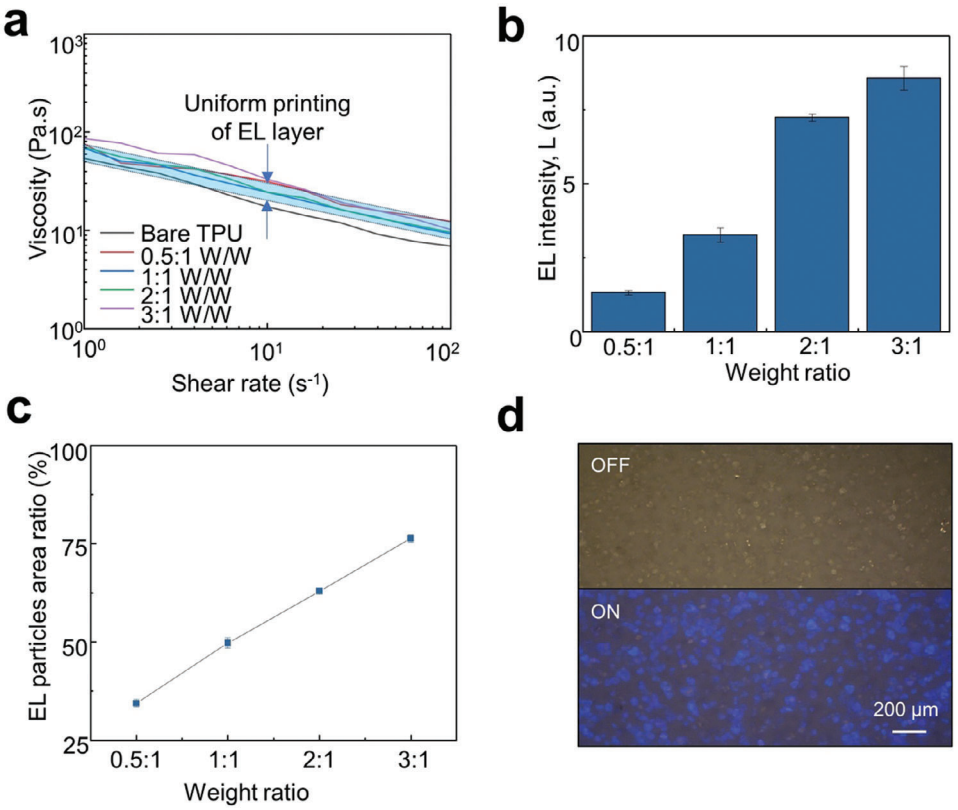

Figure 2. a) Shear rate dependence of the viscosity of ZnS phosphor/TPU slurries. b) Weight ratio dependence of EL intensity with respect to ZnS phosphors and TPU. c) Area percentage of ZnS phosphors and TPU. d) Off/on states of the EL device.

2.3. Electrical and Mechanical Characterization of Electrode Layers

Figure 3a shows the relative resistance changes of the top and bottom electrode layers during 10 000 stretching cycles at a tensile strain of 20%. Both electrodes can be regarded as resistors, with resistance typically determined by their geometric shape. According to the formula $R = \rho L \bullet S^{-1}$ (where R is resistance, ρ is resistivity, L is length, and S is cross-sectional area), upon stretching, the length increases and the cross-sectional area decreases, leading to an increase in resistance.[33] The top and bottom electrode layers maintain excellent stability and durability under repeated mechanical strain. The gradual increase in resistance after 10 000 tensile cycles could be attributed to microstructural changes, such as the formation of microcracks or slight rearrangements of conductive pathways. These effects, while resulting in small resistance increases, do not compromise the overall performance or stability of the device. Figure 3b displays the optical transmittance of the top electrode layer as a function of wavelength, showing that it maintains a high transmittance of over 80% across the visible spectrum (400 to 800 nm). This is further demonstrated in the inset photograph, which shows the transparency of the electrode layer placed over a university logo.

The Bode plot in Figure 3c presents the impedance (|Z|) and phase angle of the top electrode layer. The plot illustrates that the impedance decreases with increasing frequency, indicating that the electrode becomes more conductive at higher frequencies. The phase angle shifts toward more negative values, reflecting capacitive behavior at lower frequencies and transitioning to resistive behavior at higher frequencies. This frequency-dependent electrical characteristic is typical for conductive hydrogels, which exhibit both ionic and electronic conductivity. The Nyquist plot in Figure 3d reveals a typical semicircular pattern, characteristic of materials with both resistive and capacitive properties. In the equivalent circuit diagram, R1 represents ionic resistance, R2 represents charge transfer resistance, C represents the double-layer capacitance, and W represents diffusion-controlled impedance. The diameter of the semicircle corresponds to the charge transfer resistance, which is relatively low, indicating high ionic conductivity of the hydrogel electrode. The small diameter also confirms that the conductive hydrogel electrode maintains low resistance and reactance, making it highly suitable for applications requiring efficient charge transfer and minimal energy loss.

2.4. Light Emission Characteristics

Figure 4a shows a cross-sectional image of the PACE film, revealing its layered structure. From top to bottom, the layers are as follows: the topmost Clear Flex layer, which serves as an encapsulation layer, providing protection for the underlying functional layers. With its high optical transparency (> 98% from 400

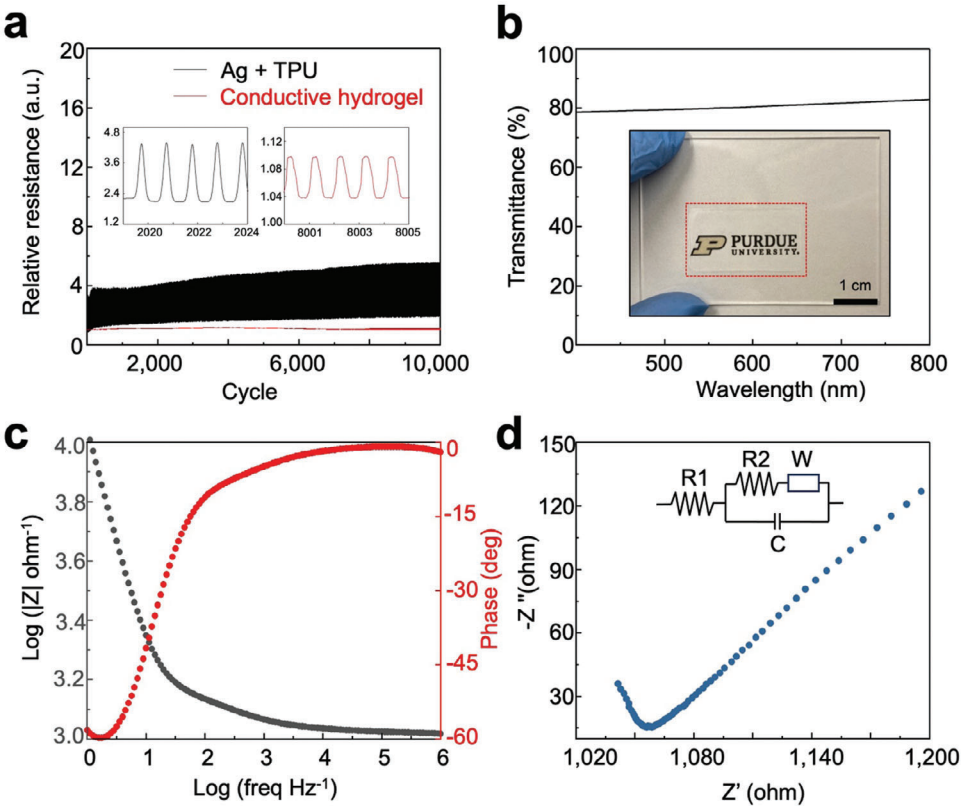

Figure 3. a) Relative resistance changes of the top and bottom electrode layers during 10 000 stretching cycles at a tensile strain of 20%. b) Optical transmittance of the top electrode layer. c) Bode plot for the top electrode layer. d) Nyquist plot for the top electrode layer.

to 800 nm), the Clear Flex layer has minimal impact on the EL intensity (Figure S3, Supporting Information). Below this layer is the conductive hydrogel electrode, visible as a dark layer. Next is the active EL layer, which contains phosphor particles responsible for the electroluminescent properties of the device. Beneath the active layer is a thin, white $BaTiO_3$ dielectric layer. Under this, a shiny grey Ag/TPU layer functions as the bottom electrode. Finally, the bottommost TPU layer acts as another encapsulating layer, completing the device's protective structure. The total thickness of the PACE film is ≈150 µm.

Figure 4b demonstrates how varying the AC voltage (30 to 180 V) and frequency (2 to 20 kHz) affects EL luminance. As the frequency increases at a fixed voltage of 180 V (6 V μm^{-1}), the light emission intensity steadily rises, resulting in a luminance increase from 77.6 to 180.98 cd m^{-2}. Beyond a certain threshold voltage, the likelihood of electrons being accelerated to excite luminescent centers increases rapidly, causing a sharp escalation in EL intensity. The experimental data align well with the fitting curves derived from the relationship between EL luminance and the applied voltage at a given frequency, as expressed by the following equation:

$$L = L_0 \exp\left(-\frac{\beta}{V^{1/2}}\right) \quad (1)$$

where L represents the luminance, V represents the applied voltage, and L_0 and β are constants determined by the EL layer. Figure 4c compares the EL intensity as a function of the thickness of both the $BaTiO_3$ and EL layers, showing how variations in layer thickness impact electroluminescent brightness. Both data series reveal a similar trend: increasing the thickness of either the EL or $BaTiO_3$ layer leads to a reduction in brightness. In the experiments, different thicknesses were achieved by adjusting the printing pressure and speed, with detailed cross-sectional images in Figure S4 (Supporting Information). The dependence of EL intensity on the weight ratio of $BaTiO_3$ to TPU is shown in Figure S5a (Supporting Information), indicating that EL intensity increases with higher weight ratios, reaching saturation at a 3:1 ratio. A comparison of EL intensity with and without the $BaTiO_3$ layer, shown in Figure S5b (Supporting Information), shows that the dielectric layer only slightly reduces EL intensity. This can be explained by the dielectric properties of the particle layer, which control the electric field distribution when voltage is applied. A matrix with a high dielectric constant focuses the electric field on the EL particles, enhancing charge separation and thus increasing light emission.[34] While the dielectric layer is not strictly necessary to prevent short circuits—since the electrode layers do not come into direct contact with the complete film—it is required for patterned structures to avoid short circuits. To maintain consistency, we included the $BaTiO_3$ layer in all configurations. Based on these results, the optimal thicknesses of 30 µm for the EL layer and 10 µm for the $BaTiO_3$ layer were selected to maximize electroluminescent intensity. The EL layer's optimized thickness is ≈30 µm due to the ZnS phosphor's

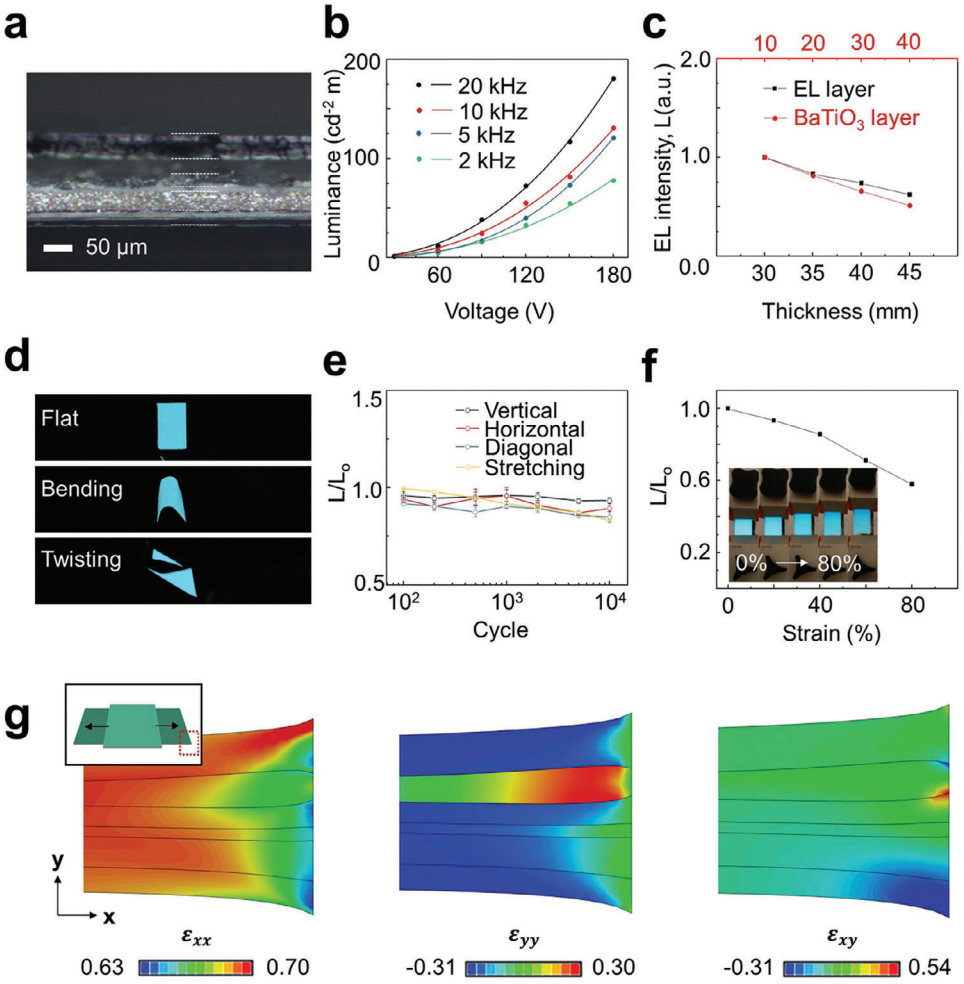

Figure 4. a) Cross-sectional image of the six-layer structure, from top to bottom: Clear Flex layer, conductive hydrogel layer, EL layer, dielectric layer, bottom electrode layer, TPU layer. b) Luminance variation in response to applied voltages at different frequencies (circles) and corresponding fitting curves (lines). c) Thickness dependence of EL intensity with respect to the EL and dielectric layers. d). Photographs of the EL device in flat and bending states. e) Relative EL intensity during 10 000 cycles of vertical, diagonal, and horizontal folding and stretching at a tensile strain of 20%. Error bars represent standard deviation, n = 3 for each group. f) Relative EL intensity upon strain. g) Interfacial shear strain distribution along the stretching direction.

average particle size (≈20.6 μm), as further reduction would cause uneven particle distribution, compromising electroluminescence. The $BaTiO_3$ layer's optimized thickness is ≈10 μm, as thinner layers pose printing challenges, such as non-uniform drying, leading to uneven thickness and reduced dielectric layer uniformity. These thicknesses ensure a balance between performance and manufacturability.

Figure 4d demonstrates the stable performance of the PACE film under various mechanical deformations, including twisting and bending (Movie S2, Supporting Information). The relative luminance (L/L_0) remained above 80% after 10 000 cycles of folding in vertical, diagonal, and horizontal directions, as shown in Figure 4e. Its response to uniaxial strain was tested by stretching the specimens until failure (Movie S3, Supporting Information), with failure occurring at 180% of the original length (Figure S6, Supporting Information). As the specimens were stretched, the intensity (emission/area) decreased, explaining the reduction in light emission. In terms of the device's long-term performance (Figure S7, Supporting Information), the PACE film maintains luminance during a 10 000 on-off cyclic test, moreover, the luminance can sustain above 80% throughout a continuous operation span of 100 h. Although thermal degradation/material fatigue will inherently reduce the brightness, a reduction in the operational frequency or surface coating of phosphor particles can be a potential approach to further extend the longevity of the devices.[35] Figure 4g illustrates the strain distribution along the stretching direction, revealing non-uniform deformation at the edges of the PACE film due to the inhomogeneous mechanical properties of the multilayer structure. The second layer, an electrode made of conductive hydrogel, expands in a direction perpendicular to the stretching direction, while the other layers contract. Typically, materials with a positive Poisson's ratio contract perpendicularly to the stretching axis, but the electrode layer—having an elastic modulus less than 15% that of the other layers—is constrained by the contraction of the adjacent upper and lower layers. This results in the electrode layer

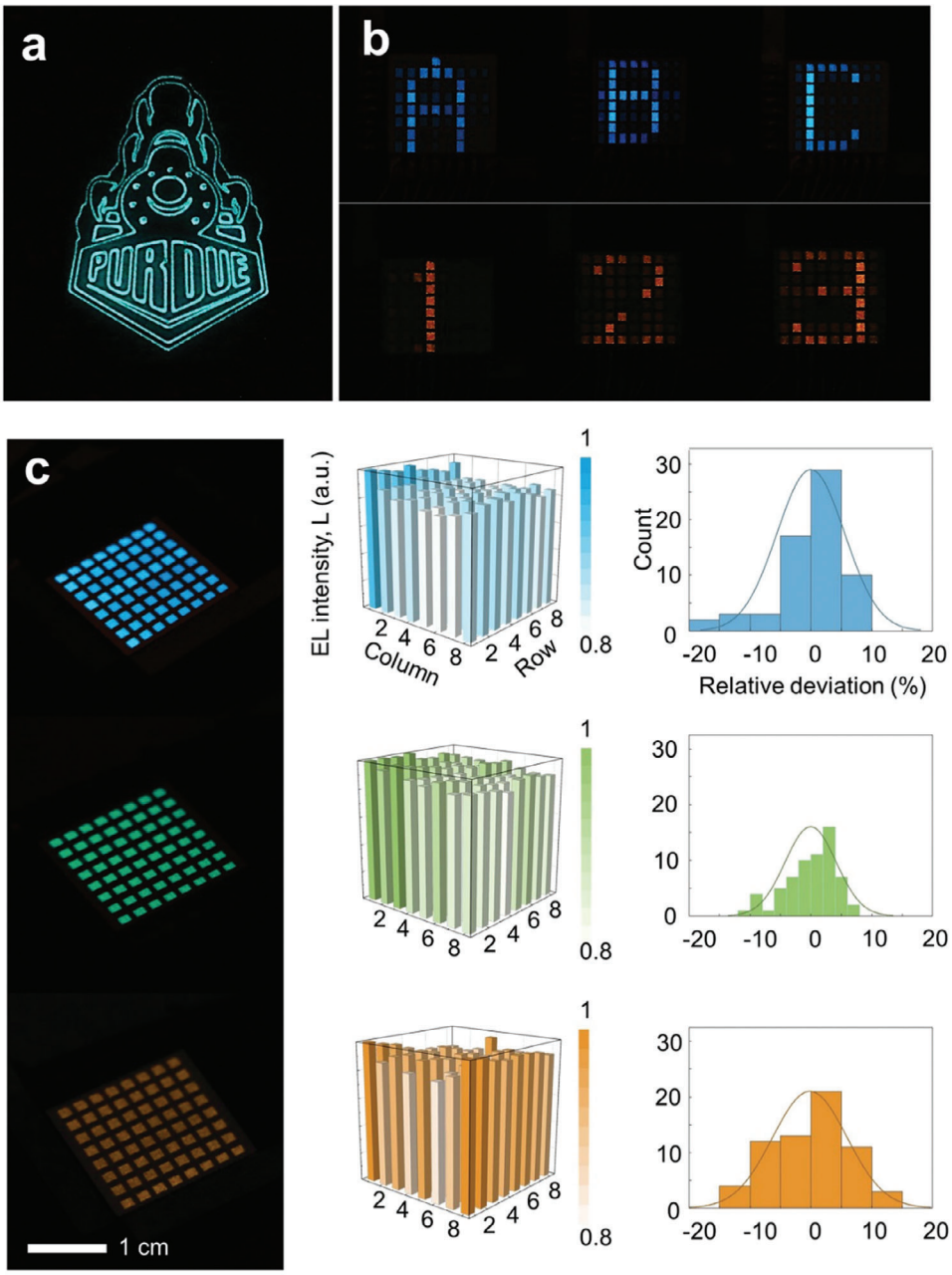

Figure 5. a) A university logo. b) Letters and numbers. c) Variation in EL intensity for different colors of EL emission.

expanding under tension, as it is strongly restricted by the adjacent layers, which have an elastic modulus over ten times greater. This expansion near the edges causes twisting and introduces opposite shear strain signs at the interfaces between the electrode layer and adjacent layers. In contrast, under bending or twisting deformation, the principal strain is significantly smaller than under tensile loading, and the shear strain at the edges is negligible compared to that observed under tensile deformation (Figure S8, Supporting Information). This observation aligns with the intensity reduction observed exclusively under tensile strain.

2.5. Proof-of-Concept Demonstrations and Pixel Control of the PACE Film

Figure 5 showcases proof-of-concept demonstrations of the PACE film. In Figure 5a, the device successfully displays a detailed pattern of a university logo (Movie S4, Supporting Information), clearly visible and illuminated, demonstrating its ability to render intricate, high-resolution designs. This highlights its potential for creating custom luminescent graphics. For a multiplexed display, passive matrix electronic addressing was employed to control light emission from 64 pixels within a 2×2 cm^2

area (Figure 5b). The relative deviations in emission intensity across all colors varied by less than 10%, confirming uniform pixel formation through the printing process (Figure 5c). This technique allows for control of an m × n matrix with only m + n control inputs, enabling the operation of all 64 pixels with just 16 relays (Figure S9, Supporting Information). The passive matrix addressing further allows the PACE film to display more complex designs, such as sweeping pixel patterns (Movie S5, Supporting Information) and alphanumeric characters (Movie S6, Supporting Information). Occasionally, unwanted pixels may activate due to the ghosting effect,[36] which reduces pixel contrast. However, this can be mitigated by using a circuit driver that controls voltage, frequency, and waveforms, ensuring high contrast in the EL pixels.[37,38] These demonstrations illustrate the versatility of the PACE film in displaying both intricate designs and simple alphanumeric characters. The ability to create clear, detailed patterns on an 8 × 8 matrix underscores its potential applications in areas such as signage, displays, and custom luminescent designs.

3. Conclusion

In this study, we introduce a new approach to printing multicolor EL films for flexible displays using a commercial dispenser system. Unlike traditional printing methods including screen printing, our refined technique is well-suited for creating custom designs. It offers precise control over the printing process, allowing for the development of intricate patterns and high-resolution displays that are difficult to achieve with conventional methods. Our method supports high-density pixel printing while maintaining consistent luminescence, with relative deviations of less than 10%. This uniformity in brightness is crucial for display applications that require high precision and clarity. Additionally, the printed films exhibit outstanding durability, enduring over 10 000 folding cycles without any significant loss in performance. The films also maintain their functionality up to 180% elongation, making them ideal for wearable electronics and other applications that require flexibility under mechanical strain.

The versatility of these printed EL films is further enhanced by their adjustable colors and luminescent intensities, enabling the creation of displays with a wide range of color outputs suitable for different environmental conditions and user preferences. The use of programmable pixels adds another layer of flexibility, allowing for dynamic and interactive displays that can be tailored to specific applications such as real-time data visualization and interactive user interfaces.

Future research could explore the use of a wider variety of materials, the addition of more color options, and the integration of these films into more complex systems, further expanding their potential. By addressing the limitations of traditional fabrication techniques and leveraging the unique benefits of a mask-free, direct-write printing process, our work not only advances the development of flexible EL devices but also opens up new possibilities for their application in a range of cutting-edge technologies.

4. Experimental Section

Fabrication of the PACE Film: A mixture of 6 mL tetrahydrofuran (Thermo Fisher Scientific) and 2 mL *N*,*N*'-dimethylformamide (Thermo Fisher Scientific) was used to dissolve 2 g thermoplastic polyurethane (TPU) pellets (Elastollan 60A, BASF) to make the TPU solution. The TPU solution was then mixed with 8 g silver flake (Inframat Advanced Materials) to create the Ag/TPU slurry. Additionally, the TPU solution was combined with 8, 9, or 10 g $BaTiO_3$ (US Research Nanomaterials, Inc.) to form the $BaTiO_3$/TPU slurry. To prepare the EL slurry, the TPU solution was mixed with 1, 2, 4, or 6 g of commercially available zinc sulfide (ZnS) phosphors with different dopants (Shanghai Keyan Phosphor Technology Co.). All slurries were mixed using a planetary centrifugal mixer (ARE-310; Thinky) at 2000 rpm for 5 min. To make the conductive hydrogel solution, 1 g PVA (MW ≈19500; Aldrich) and 0.1 g PEO (MW 100 000–200 000; Acros Organics) were dissolved in 10 mL deionized water and magnetically stirred at 170 °C for 30 min, then left at room temperature overnight. Simultaneously, 4 g LiCl (Fisher Chemical) was dissolved in 6 mL deionized water, and 1 mL of this LiCl aqueous solution was added to the PVA/PEO solution. Clear Flex (Smooth-On, Inc) solution was prepared by mixing part A and part B in a weight ratio of 1:1. All resulting slurries and solutions were then loaded into syringes with a tip diameter of 250 µm for sequential printing using a dispenser (Nordson EFD Pro 4). The glass substrate was treated with octadecyltrichlorosilane (OTS) aqueous solution at a ratio of 0.1 v/v %. After each layer was printed, it was dried in an oven at 60 °C for 1 h before proceeding to print the next layer. The conductive hydrogel and Clear Flex layers were left at room temperature overnight. Finally, the PACE film was obtained and peeled off from the glass. The viscosities of each printed material are presented in Figure S10 (Supporting Information).

Measurement of Rheological Properties: The rheological properties of all slurries and solutions were measured at room temperature using a rotational rheometer (Discovery HR-3, TA Instruments, USA) equipped with a 25 mm parallel plate (ETC Steel-115551). Measurements were conducted through a steady-state flow step at a shear rate ranging from 1.0 to 100 s^{-1}.

Characterizations of the PACE Film: Photographs and videos were captured using a digital camera (EOS 70D; Canon) equipped with an 18–135 mm lens. The surface and cross-sectional structure of the film were examined using an optical microscope (Eclipse LV150N; Nikon). The impedance of the conductive hydrogel was measured using a potentiostat (Bio-Logic SP-200). To measure the electrical properties of the conductive hydrogel and Ag/TPU under cyclic tests, a source meter (Keithley 2400) and a custom-built LabView code (National Instruments) were used in a two-wire configuration. The transmittance was characterized using an ultraviolet-visible spectrophotometer (Cary 6000i UV–vis–NIR) to scan the wavelength range of 400–800 nm. The luminance of the light-emitting pixels was measured using a chroma meter (CS-200; Konica Minolta, Japan) under an alternating sine voltage supplied by an arbitrary waveform generator (Keithley 3390) connected to a high-voltage power amplifier (9100A-DST; Tabor Electronics). All bending, folding, and stretching tests were conducted using a mechanical testing machine (Mark-10; Willrich Precision Instruments).

Finite Element Analysis (FEA): The commercially available software ABAQUS was used to analyze the deformation behavior of the PACE film. The multilayered film structure was modeled based on thicknesses measured from actual samples, with the top layers having thicknesses of 35, 25, 30, 10, 30, and 20 µm, respectively. Mechanical properties were defined using a hyperelastic model, specifically the Neo-Hookean model, with input from uniaxial tension test data and a Poisson's ratio set to 0.45. The mesh was refined to include 30 elements in the thickness direction, ensuring sufficient resolution for capturing deformation behavior across the film. The element type used was C3D8R and enhanced hourglass control was applied to improve accuracy and reduce numerical artifacts. Stretching, bending, and twisting deformations were applied by imposing displacement boundary conditions on both ends of the sample. Strain values exceeding the maximum and minimum contour limits were colored red and blue, respectively, to enhance visual analysis.

Supporting Information

Supporting Information is available from the Wiley Online Library or from the author.

Acknowledgements

This work was partly supported by the Korea Institute for Advancement of Technology (KIAT) grant, funded by the Korea Government (MOTIE) (Global Industrial Technology Cooperation Center support program and International Cooperative R&D program (P0028319)). C.H.L. also acknowledges support from the Leslie A. Geddes Endowment.

Conflict of Interest

The authors declare no conflict of interest.

Author Contributions

T.Y. and S.C. contributed equally to this work. C.H.L. supervised the project. T.Y., S.C., and C.H.L. conceived the concept. T.Y. and S.C. conducted the experiments. T.Y. and C.H.L. wrote the manuscript. J.L. conducted the FEA simulation. Z.W. contributed to data collection and the preliminary experiments. All authors contributed to the analysis and discussion of the data.

Data Availability Statement

The data that support the findings of this study are available from the corresponding author upon reasonable request.

Keywords

conductive hydrogels, displays, electroluminescent devices, printable electronics, stretchable electronics

Received: November 15, 2024
Revised: January 2, 2025
Published online:

[1] H. Yin, Y. Zhu, K. Youssef, Z. Yu, Q. Pei, *Adv. Mater.* **2022**, *34*, 2106184.
[2] R. Shanker, S. Cho, A. Choe, M. P. Kim, Z. Khan, S. Kang, H. Ko, *Adv. Funct. Mater.* **2019**, *29*, 1904377.
[3] G. Li, F. Sun, S. Zhao, R. Xu, H. Wang, L. Qu, M. Tian, *Nano Lett.* **2023**, *23*, 8436.
[4] P. Fu, J. Li, M. Zhong, J. Huang, R. Tan, W. Song, *ACS Appl. Opt. Mater.* **2024**, *2*, 816.
[5] W. Yang, S. Lin, W. Gong, R. Lin, C. Jiang, X. Yang, Y. Hu, J. Wang, X. Xiao, K. Li, Y. Li, Q. Zhang, J. S. Ho, Y. Liu, C. Hou, H. Wang, *Science* **2024**, *384*, 74.
[6] X. Shi, Y. Zuo, P. Zhai, J. Shen, Y. Yang, Z. Gao, M. Liao, J. Wu, J. Wang, X. Xu, *Nature* **2021**, *591*, 240.
[7] Y. Zuo, X. Shi, X. Zhou, X. Xu, J. Wang, P. Chen, X. Sun, H. Peng, *Adv. Funct. Mater.* **2020**, *30*, 2005200.
[8] S. Cho, T. Chang, T. Yu, S. L. Gong, C. H. Lee, *Sci. Adv.* **2024**, *10*, eadk4295.
[9] J. He, R. Wei, X. Ma, W. Wu, X. Pan, J. Sun, J. Tang, Z. Xu, C. Wang, C. Pan, *Adv. Mater.* **2024**, *36*, 2401931.
[10] W. Liu, C. Zhang, R. Alessandri, B. T. Diroll, Y. Li, H. Liang, X. Fan, K. Wang, H. Cho, Y. Liu, Y. Dai, Q. Su, N. Li, S. Li, S. Wai, Q. Li, S. Shao, L. Wang, J. Xu, X. Zhang, D. V. Talapin, J. J. de Pablo, S. Wang, *Nat. Mater.* **2023**, *22*, 737.
[11] D. C. Kim, H. Seung, J. Yoo, J. Kim, H. H. Song, J. S. Kim, Y. Kim, K. Lee, C. Choi, D. Jung, C. Park, H. Heo, J. Yang, T. Hyeon, M. K. Choi, D.-H. Kim, *Nat. Electron.* **2024**, *7*, 365.
[12] L. Yin, M. Cao, K. N. Kim, M. Lin, J.-M. Moon, J. R. Sempionatto, J. Yu, R. Liu, C. Wicker, A. Trifonov, F. Zhang, H. Hu, J. R. Moreto, J. Go, S. Xu, J. Wang, *Nat. Electron.* **2022**, *5*, 694.
[13] Z. Zhang, *Nat. Rev. Mater.* **2022**, *7*, 839.
[14] V. Wang, S. Z. Uddin, J. Park, A. Javey, *Sci. Adv.* **2023**, *9*, eadg1607.
[15] H. Jinno, T. Yokota, M. Koizumi, W. Yukita, M. Saito, I. Osaka, K. Fukuda, T. Someya, *Nat. Commun.* **2021**, *12*, 2234.
[16] Y. Go, H.-Y. Park, Y. Zhu, K. Yoo, J. Kwak, S.-H. Jin, J. Yoon, *Adv. Funct. Mater.* **2023**, *33*, 2215193.
[17] P. Zhang, I. M. Lei, G. Chen, J. Lin, X. Chen, J. Zhang, C. Cai, X. Liang, J. Liu, *Nat. Commun.* **2022**, *13*, 4775.
[18] J. Zhang, Q. Lu, M. Wu, Y. Sun, S. Wang, X. Wang, M.-H. Lu, D. Kong, *npj Flexible Electron.* **2024**, *8*, 1.
[19] Z. Zhang, Z. Bao, *Natl. Sci. Rev.* **2023**, *10*, nwac093.
[20] F. Ma, Y. Lin, W. Yuan, C. Ding, W. Su, X. Meng, Z. Cui, *ACS Appl. Electron. Mater.* **2021**, *3*, 1747.
[21] H. Guo, Y. Lin, S. Gu, G. Hu, Q. Wang, C. Bai, Y. Sun, C. Yang, T. Fang, X. Chen, D. Li, D. Kong, *Nano Lett.* **2024**, *24*, 5904.
[22] Y. Lin, X. Chen, Q. Lu, J. Wang, C. Ding, F. Liu, D. Kong, W. Yuan, W. Su, Z. Cui, *ACS Appl. Mater. Interfaces* **2023**, *15*, 5931.
[23] Z. Luo, W. Chen, M. Lai, S. Shi, P. Chen, X. Yang, Z. Chen, B. Wang, Y. Zhang, X. Zhou, *Adv. Mater.* **2024**, *36*, 2313909.
[24] S. Li, B. N. Peele, C. M. Larson, H. Zhao, R. F. Shepherd, *Adv. Mater.* **2016**, *28*, 9770.
[25] B. H. Kim, S. Nam, N. Oh, S.-Y. Cho, K. J. Yu, C. H. Lee, J. Zhang, K. Deshpande, P. Trefonas, J.-H. Kim, J. Lee, J. H. Shin, Y. Yu, J. B. Lim, S. M. Won, Y. K. Cho, N. H. Kim, K. J. Seo, H. Lee, T.-i. Kim, M. Shim, J. A. Rogers, *ACS Nano* **2016**, *10*, 4920.
[26] H. Lee, D.-h. Kang, S. Cho, Y.-R. Kim, Y. Lee, S. Na, H. Cho, S. Lee, G. Lim, J. Yeom, H. Ko, *ACS Appl. Mater. Interfaces* **2023**, *15*, 16299.
[27] X. Xu, D. Hu, L. Yan, S. Fang, C. Shen, Y.-L. Loo, Y. Lin, C. S. Haines, N. Li, A. A. Zakhidov, H. Meng, R. H. Baughman, W. Huang, *Adv. Mater.* **2017**, *29*, 1703552.
[28] C. Zhao, Y. Zhou, S. Gu, S. Cao, J. Wang, M. Zhang, Y. Wu, D. Kong, *ACS Appl. Mater. Interfaces* **2020**, *12*, 47902.
[29] Y. Zhang, X. Wang, Y. Zhang, M. Liu, Z. Zhao, Z. Shen, Y. Hu, *Adv. Funct. Mater.* **2024**, *34*, 2308969.
[30] A. Haake, R. Tutika, G. M. Schloer, M. D. Bartlett, E. J. Markvicka, *Adv. Mater.* **2022**, *34*, 2200182.
[31] K. Sim, S. Chen, Z. Li, Z. Rao, J. Liu, Y. Lu, S. Jang, F. Ershad, J. Chen, J. Xiao, C. Yu, *Nat. Electron.* **2019**, *2*, 471.
[32] C. Larson, B. Peele, S. Li, S. Robinson, M. Totaro, L. Beccai, B. Mazzolai, R. Shepherd, *Science* **2016**, *351*, 1071.
[33] X. Zhang, J. Zhang, W. Liao, D. Zhang, Y. Dai, C. Wu, J. Wen, W. Zeng, *J. Mater. Chem. C* **2023**, *11*, 15873.
[34] F. Stauffer, K. Tybrandt, *Adv. Mater.* **2016**, *28*, 7200.
[35] F. Chun, B. Zhang, Y. Gao, X. Wei, Q. Zhang, W. Zheng, J. Zhou, Y. Guo, X. Zhang, Z. Xing, X. Yu, F. Wang, *Nat. Photon.* **2024**, *18*, 856.
[36] O. Amiraslanov, P. Lukowicz, J. Cheng, in *Proceedings of the 2016 ACM International Joint Conference on Pervasive and Ubiquitous Computing: Adjunct*, Association for Computing Machinery, Heidelberg, Germany **2016**.
[37] A. Ivanov, A printed electroluminescent matrix display: implementation details and technical solutions in 2018 IMAPS Nordic Conference on Microelectronics Packaging (NordPac), (ieee, **2018**), pp. 86-94.
[38] S. Yun, S.-K. Lee, B. Allabergenov, J. C. Park, S. Moon, S. E. Lee, B. Choi, *Adv. Photonics Res.* **2023**, *4*, 2200291.